BIOPHYSICS

Photophysics-informed two-photon voltage imaging using FRET-opsin voltage indicators

F. Phil Brooks III†, Daozheng Gong†, Hunter C. Davis†, Pojeong Park, Yitong Qi, Adam E. Cohen*

Microbial rhodopsin–derived genetically encoded voltage indicators (GEVIs) are powerful tools for mapping bioelectrical dynamics in cell culture and in live animals. Förster resonance energy transfer (FRET)–opsin GEVIs use voltage-dependent quenching of an attached fluorophore, achieving high brightness, speed, and voltage sensitivity. However, the voltage sensitivity of most FRET-opsin GEVIs has been reported to decrease or vanish under two-photon (2P) excitation. Here, we investigated the photophysics of the FRET-opsin GEVIs Voltron1 and Voltron2. We found that the previously reported negative-going voltage sensitivities of both GEVIs came from photocycle intermediates, not from the opsin ground states. The voltage sensitivities of both GEVIs were nonlinear functions of illumination intensity; for Voltron1, the sensitivity reversed the sign under low-intensity illumination. Using photocycle-optimized 2P illumination protocols, we demonstrate 2P voltage imaging with Voltron2 in the barrel cortex of a live mouse. These results open the door to high-speed 2P voltage imaging of FRET-opsin GEVIs in vivo.

INTRODUCTION

Genetically encoded voltage indicators (GEVIs) are a powerful class of fluorescent probes for mapping bioelectrical signals (*1*). These tools have been used in multiple species (*2*–*7*) and at levels of biological organization from subcellular (*8*–*10*) to organ-wide (*11*–*13*). Microbial rhodopsin–based GEVIs have fast (submillisecond) responses to voltage steps and good voltage sensitivity (*14*, *15*). The first opsin-based GEVIs relied on the near-infrared fluorescence of the retinal cofactor, but this signal was very dim (*5*, *14*, *16*). In Förster resonance energy transfer (FRET)–opsin GEVIs, voltage-dependent changes in the efficiency of FRET from an attached fluorophore to the opsin lead to modulation of the fluorophore brightness (Fig. 1A) (*17*, *18*). This approach has been demonstrated with fusions of fluorescent proteins to microbial rhodopsins (*7*, *19*) and with fusions of the HaloTag receptor, which can be covalently loaded with a small-molecule organic dye (*2*, *20*). FRET-opsin GEVIs are fast, bright, and sensitive (*2*, *17*, *20*–*22*).

A key challenge in voltage imaging is to resolve signals within light-scattering tissues, such as the brain. Most applications of voltage imaging to date have used one-photon (1P) excitation. While structured illumination, far-red excitation, and the use of photoactivatable GEVIs can partially reduce the background from scattered light (*23*), 1P voltage imaging is still limited to imaging the top ~250 μm of brain tissue. Two-photon (2P) excitation has been transformative for calcium imaging in vivo, so there has been substantial interest in developing 2P voltage imaging systems (*24*, *25*). The FRET-opsin GEVIs would be attractive targets for 2P voltage imaging, but for reasons that have remained mysterious, most FRET-opsin GEVIs show little or no voltage sensitivity under typical 2P illumination conditions, even when the fluorescence count rate is high enough that voltage-induced fluorescence changes should be detectable (*26*, *27*). Furthermore, these same samples can return to showing voltage sensitivity under 1P illumination after 2P illumination (*26*). These observations led us to explore the photophysical basis of voltage sensitivity in FRET-opsin GEVIs.

In the simplest model of a FRET-opsin GEVI (Fig. 1A), a voltage-insensitive FRET donor is optically excited. The opsin FRET acceptor sits in a voltage-sensitive equilibrium between two states, one of which quenches the donor more efficiently than the other. This simple model produces two important predictions. First, the fractional response of the donor fluorescence to voltage (i.e., $\Delta F/F$ versus V) should be a function only of voltage and not of any illumination parameters. Second, any excitation method (e.g., 1P or 2P) that produces the same donor excited state should produce the same voltage-sensitive fluorescence signal. The documented failure of 2P voltage imaging with FRET-opsin GEVIs suggests that this simple picture is inadequate.

The light used to excite the FRET donor can also interact with the opsin acceptor directly (Fig. 1B). Microbial rhodopsins have complex photocycles, with at least seven spectroscopically distinguishable states, and a variety of light- and voltage-modulated transitions (*28*–*33*). Illumination with pulses of light of tuned wavelength and intensity can shift the opsin population among these states. The complexity of opsin photocycles has been harnessed to create light-gated voltage integrators (*34*), light-gated voltage sample-and-hold motifs (*34*), reporters of absolute voltage (*35*), and photoactivated voltage indicators (*23*). Each opsin scaffold and mutant can have distinct photocycle dynamics.

In wild-type Archaerhodopsin 3 (Arch), voltage-sensitive retinal fluorescence comes from a photocycle intermediate termed the "Q state," not from the dark-adapted ground state. Exciting voltage-sensitive fluorescence requires sequential absorption of three photons, leading to an illumination intensity–dependent increase in voltage sensitivity (*23*, *31*). The engineering of Arch-based voltage sensors such as the QuasAr and Archon variants eliminated the requirement for sequential multiphoton excitation (*33*, *36*, *37*). FRET-opsin GEVIs are most often based on a different opsin scaffold, derived from *Acetabularia*. To our knowledge, there have been no studies of how or whether photocycle dynamics affect the function of FRET-opsin GEVIs. In the initial characterizations (*2*, *17*, *18*, *20*) and subsequent applications (*8*, *10*, *19*, *38*) of these reporters, there is an implicit assumption that the voltage sensitivity emerges from the photocycle ground states.

Department of Chemistry and Chemical Biology, Harvard University, Cambridge, MA, USA.
*Corresponding author. Email: cohen@chemistry.harvard.edu
†These authors contributed equally to this work.

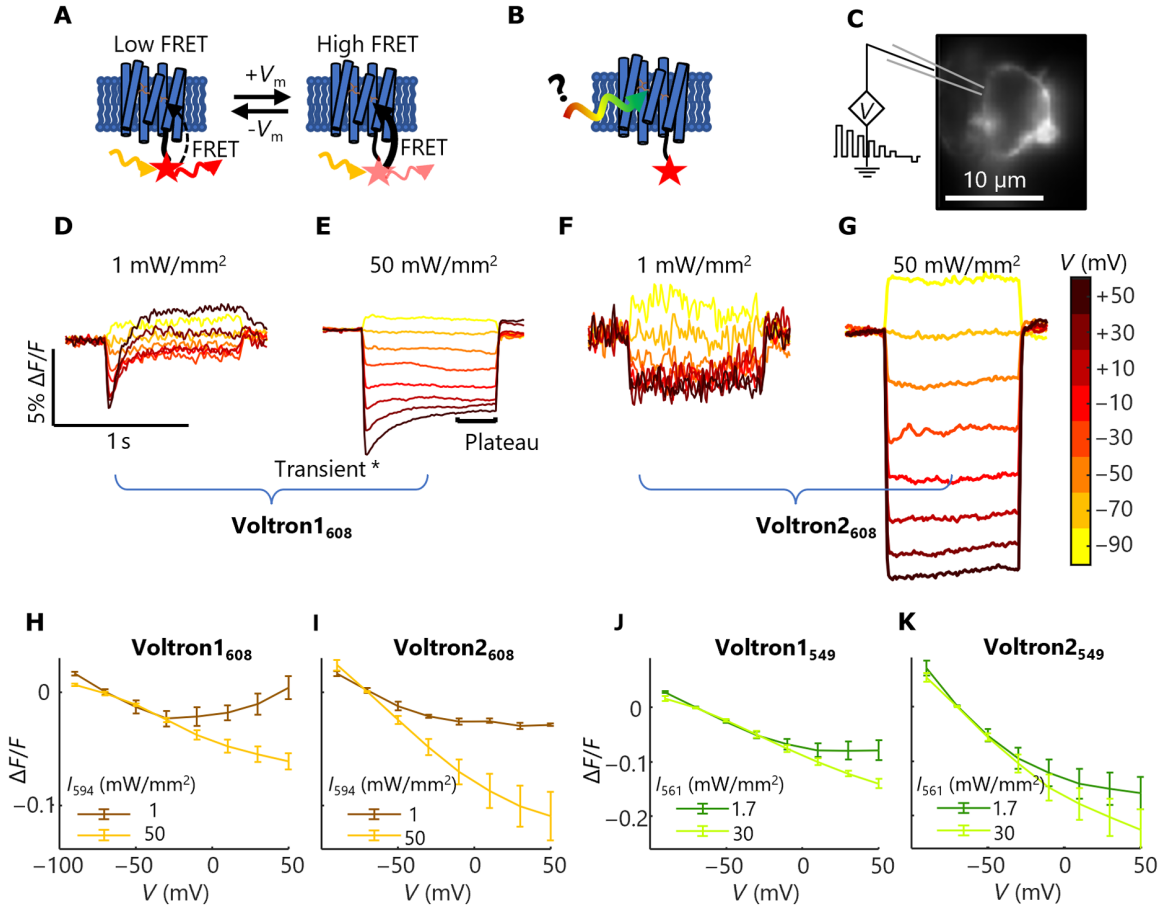

Fig. 1. Illumination-dependent performance of FRET-opsin voltage indicators. (**A**) Simple model of a FRET-opsin GEVI. A fluorescent FRET donor is optically excited and can relax either by fluorescence or by FRET to the retinal chromophore. Voltage-dependent shifts in the retinal absorption spectrum modulate the fluorescence of the donor. (**B**) The light used to excite the FRET donor may also excite the retinal chromophore directly, driving phototransitions in the opsin and changing the voltage-sensing properties of the GEVI. (**C**) Fluorescence image of a HEK-293T cell expressing Voltron2$_{608}$ and subject to voltage clamp. (**D** and **E**) Voltage step responses from cells expressing Voltron1$_{608}$ at low (1 mW/mm^2) and high (50 mW/mm^2) illumination intensities at $\lambda = 594$ nm. Transient and plateau phases of the response are indicated. At low intensity, steady-state fluorescence responses showed a nonmonotonic dependence on membrane voltage. (**F** and **G**) Same as (D) and (E) for Voltron2$_{608}$, with the same $\Delta F/F$ vertical scale. (**H** to **K**) Plots of steady-state $\Delta F/F$ versus V for (H) Voltron1$_{608}$, (I) Voltron2$_{608}$, (J) Voltron1$_{549}$, and (K) Voltron2$_{549}$. Each curve is plotted for dim (dark colors) and bright (light colors) illumination. For all reporter combinations, both the slope and shape of the curve were sensitive to illumination intensity. Error bars represent SEM from three to six cells.

Here, we hypothesized that the voltage-sensing properties of FRET-opsin GEVIs might also depend in a complex way on the intensity, wavelength(s), and time course of illumination and that an understanding of these dependencies could suggest illumination protocols that would enable 2P voltage imaging. We found that the voltage sensitivities of FRET-opsin GEVIs Voltron1 and Voltron2 depended on illumination intensity, indicating that the previously reported negative-going voltage sensitivity arises from a photocycle intermediate rather than the ground state. Inspired by these photophysical data, we optimized the 2P imaging protocol and demonstrated in vivo 2P voltage imaging. These results open a path for 2P voltage imaging with FRET-opsin GEVIs in vivo.

RESULTS

We expressed Voltron1 (*20*) or Voltron2 (*2*) in human embryonic kidney (HEK) 293T cells and labeled the samples with HaloTag ligand dye JF$_{608}$ (Materials and Methods). We selected this dye because it has been useful in all-optical electrophysiology experiments with Voltron1 and Voltron2 (*8*, *10*). We then used a whole-cell voltage clamp to vary the membrane voltage, and we recorded the fluorescence under continuous 594-nm 1P illumination at different intensities (Fig. 1C).

We first applied a series of voltage steps from a holding potential of −70 mV to voltages from −90 to +50 mV (Fig. 1, D to G). At high illumination intensity (50 mW/mm^2), both GEVIs showed an approximately linear and negative-going dependence of steady-state fluorescence on membrane voltage, with slopes $\Delta F/F = -0.054 \pm 0.007$ per 100 mV (Voltron1, $n = 4$ cells) and $\Delta F/F = -0.11 \pm 0.02$ per 100 mV (Voltron2, $n = 5$ cells), where ΔF was measured relative to F at $V = -70$ mV (Fig. 1, H and I). The differences in scale between the voltage sensitivities reported here and those in prior reports (*2*, *20*) are likely due to variations in protein trafficking efficiency and analysis methods and do not affect our conclusions. For depolarizations to >0 mV, Voltron1 showed an initial transient fluorescence peak (Fig. 1E), but Voltron2 did not (Fig. 1G). These data are consistent with prior reports (*2*, *20*).

At low illumination intensity (0.97 mW/mm^2), the voltage responses of both GEVIs changed markedly. The initial transient fluorescence response of Voltron1 maintained its approximately linear negative-going dependence on voltage. However, the steady-state F versus V response of Voltron1 became nonmonotonic. For small depolarizations relative to −70 mV, the fluorescence decreased, as at high intensity. However, for depolarizations to >−20 mV, the Voltron1 fluorescence increased as voltage increased, and at voltages >+30 mV, the steady-state fluorescence was actually brighter than at $V = -70$ mV (Fig. 1, D and H). The F versus V curves at intermediate illumination intensities smoothly interpolated between the limiting cases plotted in Fig. 1.

For Voltron2 at low illumination intensity, the voltage step response maintained its top-hat structure (Fig. 1F), but the overall voltage sensitivity decreased nearly twofold for small depolarizations around −70 mV, and the voltage response leveled off for voltages >−20 mV. Qualitatively similar intensity-dependent changes in the transient and steady-state voltage responses were observed when the two GEVIs were loaded with JF_{549} and excited at 561 nm (Fig. 1, J and K).

To quantify the influence of illumination intensity on voltage sensitivity, we performed voltage-clamp experiments at 1P illumination intensities spanning nearly four orders of magnitude, from 0.06 to 100 mW/mm^2 (Fig. 2, A and B). At each intensity, we clamped the voltage at −70 mV and then measured the fluorescence responses to a 100-mV depolarizing step to +30 mV. For Voltron1, we plotted separately the initial and steady-state fluorescence responses, as marked in Fig. 1E. For Voltron2, initial and steady-state fluorescence were indistinguishable.

The data showed several unexpected features. For an idealized GEVI, one would expect both ΔF and F to be proportional to intensity and their ratio ($\Delta F/F$) to be independent of intensity. We found that for both indicators, $\Delta F/F$ depended strongly on illumination intensity. This observation shows that statements of FRET-opsin voltage sensitivity are only meaningful if illumination intensity is specified. For both GEVIs, the voltage sensitivity was the greatest (in absolute value), and the illumination intensity dependence leveled off around 10 to 30 mW/mm^2. By good fortune, this intensity regime is typically used in neural recordings because it produces high-enough per-cell count rates to observe neural dynamics over shot noise. This coincidence may explain why the low-intensity anomalous responses of these GEVIs were not previously reported.

These data also show the disparate effects of illumination intensity on different response timescales. At low illumination intensity, Voltron1 showed the unexpected inversion of steady-state sensitivity to 100-mV voltage steps (Fig. 2A). Furthermore, at low intensity, Voltron1 showed increased disparity between the transient and steady-state responses to 100-mV voltage steps. While the sensitivity of Voltron2 was in general superior to Voltron1, for illumination intensities between 1 and 10 mW/mm^2, the transient response of Voltron1 was larger than that of Voltron2.

We next sought to determine the kinetics with which voltage sensitivity increased under bright illumination and decreased under dim illumination. To measure these parameters, in HEK cells expressing either $Voltron1_{608}$ or $Voltron2_{608}$, we alternately clamped the voltage at −70 and +30 mV, and at each voltage, we applied pulses of bright light (594 nm for JF_{608} and 561 nm for JF_{549}; 75 ms, 15 mW/mm^2) interleaved with dim light (675 ms, 0.75 mW/mm^2; Fig. 2C). By comparing the fluorescence at the two voltages during the dim-to-bright and bright-to-dim transitions, we measured the onset and decay of voltage sensitivity (Fig. 2, D and E). For $Voltron1_{608}$, voltage sensitivity arose with a time constant of 5 ms and decayed with a time constant of 46 ms (Fig. 2D). For $Voltron2_{608}$, voltage sensitivity arose with a time constant of 4 ms and decayed with a time constant of 16 ms (Fig. 2E).

The appearance of the "normal" (i.e., previously reported) F versus V behavior only at high illumination intensities, along with the finite time constants for voltage sensitivity to appear in response to a stepwise increase in illumination intensity, suggested that normal Voltron voltage sensitivity might involve a photocycle intermediate, not the ground state (Fig. 2F). Sufficient 1P illumination populates the voltage-sensitive states, which then thermally relax to the dark-adapted state. The model of Fig. 2F is almost certainly an oversimplification, particularly for $Voltron1_{608}$. The nonlinear dependence of F versus V at low intensity (Fig. 1H) and the differing transient versus steady-state step responses (Figs. 1D and 2A) together imply the existence of more than one voltage-dependent transition among the photocycle intermediates. Because these effects occurred only at very low intensity and only in Voltron1, we did not pursue them further.

2P photophysics

We hypothesized that the previously reported poor 2P voltage sensitivity in opsin-based GEVIs (*26*, *39*) might arise from failure to populate voltage-sensitive photocycle intermediates (Fig. 2F). This hypothesis is consistent with our observations that sufficient 1P illumination was required to observe 1P voltage sensitivity and with the much lower per-molecule excitation rate of 2P versus 1P excitation.

JF_{549} was among the first dyes reported for use with Voltron (*20*) and has a 2P excitation peak in the center of the 1030- to 1080-nm mid-infrared window reachable by multiple femtosecond laser technologies. We expressed $Voltron2_{549}$ in HEK cells, clamped the voltage at −70 mV, and applied voltage steps from −90 to +50 mV. We first imaged the sample with donut-scanned 1040-nm 2P excitation (9.4 mW, 1-kHz scan repetition rate) and then applied the same voltage steps immediately afterward under wide-field 1P excitation (26 mW/mm^2, 532 nm). Under 2P illumination, the fractional voltage sensitivity was much smaller and the step-response kinetics were much slower compared to those under 1P illumination of the same cell (Fig. 3A). At 9.4 mW per cell, the dye bleached with a time constant of 3 s (Fig. 3A, inset). The 2P voltage sensitivity was 0.045 ± 0.012 per 100 mV ($n = 9$ cells, mean ± SEM; Fig. 3, D and E), significantly smaller than the 1P sensitivity of 0.13 ± 0.02 per 100 mV ($n = 9$ cells, mean ± SEM; Fig. 3E) from paired measurements on the same set of cells ($P = 0.0006$, two-tailed t test; Fig. 3E). Given the rapid photobleaching, it was not practical to increase the illumination intensity further to see whether the voltage sensitivity increased.

The 2P action spectrum for Voltron sensitization is not known, but prior work on 2P excitation of bacteriorhodopsin provides some guidance. For bacteriorhodopsin, 2P excitation of the S_1 first excited state peaks at 1140 nm, whereas 2P excitation to the S_2 second excited state (a symmetry-forbidden 1P transition) is a broad transition centered just under 1000 nm (*40*). Retinal isomerization and initiation of the photocycle require excitation to S_1, so we reasoned that 2P excitation to S_1 might favor voltage sensitivity, while excitation to S_2 might be unproductive or even counteract sensitization. This reasoning suggested that 2P excitation around 1140 nm might favor population of voltage-sensitive states. The JF_{608} dye shows 2P excitation with a peak around 1135 nm (*41*), so we reasoned that in

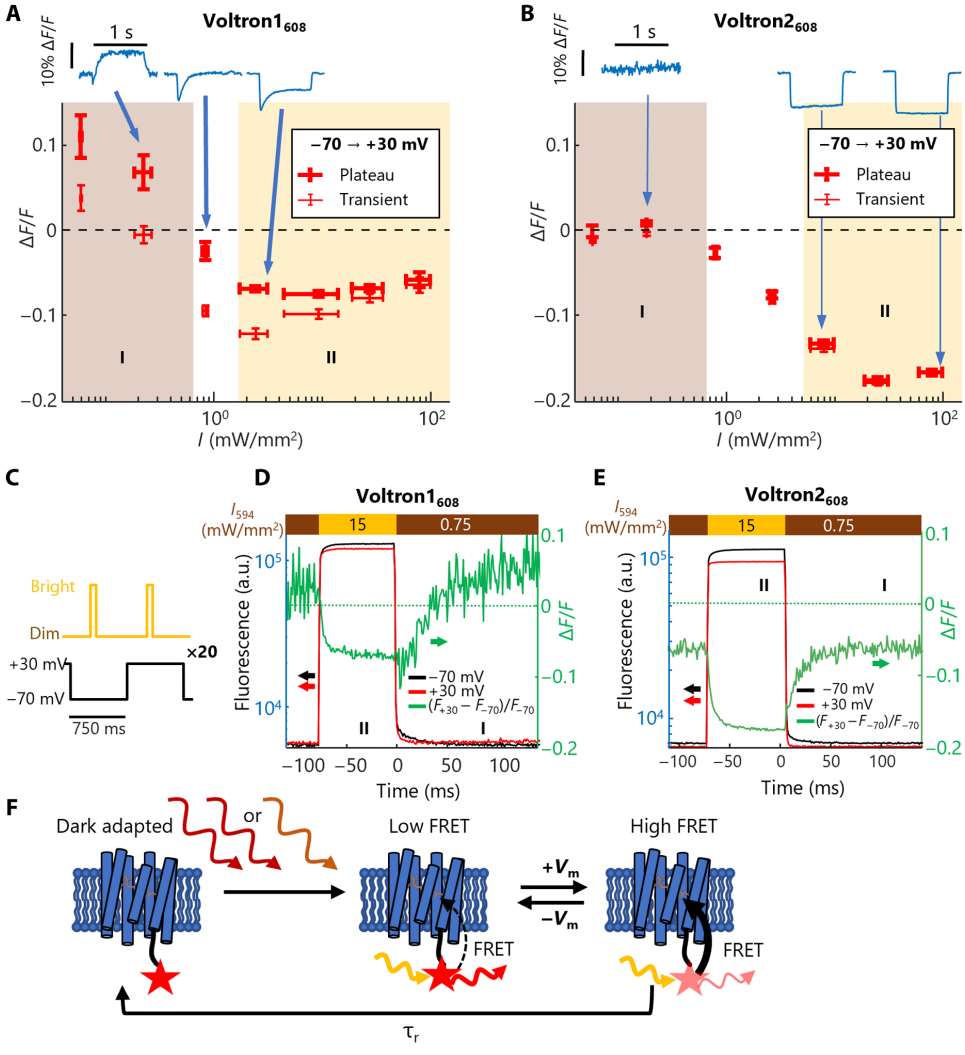

Fig. 2. Intensity-dependent voltage sensitivity of Voltron GEVIs. (**A**) Sensitivity ($\Delta F/F$) of Voltron1$_{608}$ as a function of illumination intensity for voltage steps from −70 to +30 mV ($n = 5$ cells). Horizontal error bars denote the range of illumination intensities; vertical error bars denote SEM. Blue, representative step responses. **I** and **II** mark the insensitive and voltage-sensitive regimes, respectively [also in (B), (D), and (E)]. (**B**) Same as (A), but for Voltron2$_{608}$ ($n = 3$ cells). (**C**) Protocol for measuring GEVI responses to a step in illumination. Dynamics in the "dark" were probed by very dim (0.75 mW/mm^2) illumination; bright pulses (75 ms, 15 mW/mm^2) transiently populated the voltage-sensitive states. (**D**) The voltage sensitivity of Voltron1$_{608}$ (green, right axis) was calculated from the difference between the fluorescence at −70 mV (black, left axis) and at +30 mV (red, left axis). Sensitivity emerged with a time constant of 5 ms and declined with a time constant of 46 ms. a.u., arbitrary units. (**E**) Same as (D) for Voltron2$_{608}$. Sensitivity emerged with a time constant of 4 ms and declined with a time constant of 16 ms. (**F**) Model of photoactivated voltage sensitivity in a FRET-opsin voltage indicator. Dark-adapted Voltron2 does not show voltage-dependent FRET. Upon absorption of at least one photon (e.g., 594- or 1135-nm 2P), the opsin enters a voltage-sensitive equilibrium between high- and low-FRET states. In Voltron2, this equilibrium relaxes to the dark-adapted state with a time constant $\tau_r \sim 16$ ms.

Voltron2$_{608}$, 2P light at 1135 nm might drive opsin sensitization and simultaneously excite the FRET donor for voltage imaging.

We expressed Voltron2$_{608}$ in HEK cells, clamped the voltage at −70 mV, and applied voltage steps from −90 to +50 mV under 9.5-mW 2P excitation at 1135 nm (Fig. 3, B to E). The laser scan traced the periphery of the cell membrane at 1000 Hz. We then repeated the voltage steps under moderate (6 mW/mm^2) 1P excitation at 594 nm (Fig. 3B). Under 2P excitation, Voltron2$_{608}$ showed much larger voltage sensitivity than Voltron2$_{549}$ (Fig. 3, C to E), consistent with our hypothesis that long-wavelength 2P excitation was more effective at populating the voltage-sensitive photocycle intermediate. Under 2P excitation, Voltron2$_{608}$ showed a step-response time of 2 ms at room temperature, similar to the 1P step response in Fig. 1G.

We explored the dependence of voltage sensitivity of Voltron2$_{608}$ on 2P illumination power. We applied voltage steps from −70 to +30 mV at powers ranging from 0.3 to 15 mW. As with 1P illumination, the voltage sensitivity disappeared at low illumination power and increased with illumination power, saturating at 10 mW (Fig. 3F). This observation aligns with our hypothesis that 2P voltage sensitivity requires population of voltage-sensitive photocycle intermediate states.

2P voltage imaging in vivo

Last, we tested 2P voltage imaging of Voltron2$_{608}$ in vivo. We injected a viral vector for cre-dependent bicistronic expression of Voltron2 and CheRiff into the layer 1 barrel cortex of *Ndnf-Cre* mice. We implanted

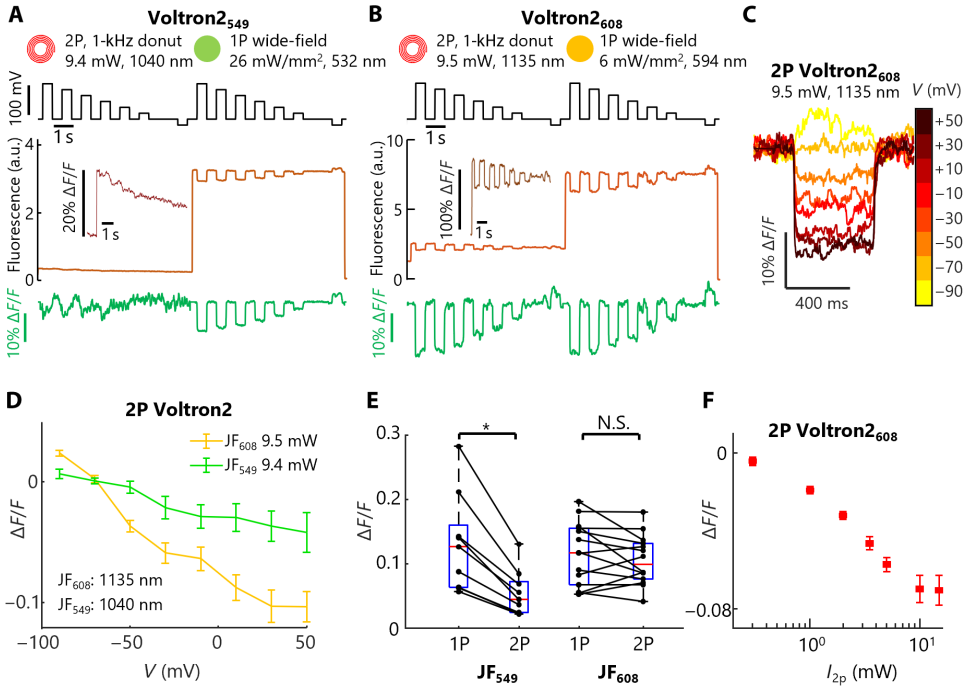

Fig. 3. 2P voltage imaging with Voltron2. (**A**) Comparison of Voltron2$_{549}$ voltage sensitivity under 2P versus 1P illumination. A HEK-293T cell expressing Voltron2$_{549}$ was subjected to voltage steps from a holding potential of −70 mV. Fluorescence was recorded under 2P excitation and then under 1P excitation. The fractional changes in fluorescence were smaller and slower under 2P versus 1P excitation. The inset shows a magnified 2P fluorescence trace. Photobleaching was corrected before calculating Δ*F*/*F*. (**B**) Same as (A), but with Voltron2$_{608}$. (**C**) Voltage step response from the same Voltron2$_{608}$-expressing cell shown in (B). (**D**) Voltage response under 2P excitation for Voltron2$_{549}$ and Voltron2$_{608}$ under bright (9.4 to 9.5 mW) illumination. Error bars represent SEM (n = 6 to 12 cells). (**E**) Comparison of responses to a 100-mV step (−90 to +10 mV) for Voltron2$_{549}$ and Voltron2$_{608}$ from matched samples and measurement conditions. Voltron2$_{549}$ 1P: 26 mW/mm^2, 532 nm; 2P: 9.4 mW, 1040 nm; n = 9 cells. Voltron2$_{608}$ 1P: 6 mW/mm^2, 594 nm; 2P: 9.5 mW, 1135 nm; n = 14 cells. Error bars represent the mean ± SEM. 1P voltage sensitivity was significantly greater than 2P voltage sensitivity for Voltron2$_{549}$ (*P = 0.0006, two-tailed t test) but not for Voltron2$_{608}$. N.S., not significant. (**F**) Fractional sensitivity (Δ*F*/*F*) of Voltron2$_{608}$ as a function of 2P illumination power for a voltage step from −70 to +30 mV. Error bars represent SEM (n = 13 to 30 cells).

cranial windows and performed optical stimulation and voltage imaging of layer 1 interneurons in anesthetized mice. We sequentially performed 2P (1135 nm, 15 to 54 mW) and 1P (594 nm, 30 mW/mm^2) imaging on the same cells while evoking neuronal spikes with pulses of 488-nm illumination (1.5 mW/mm^2; Fig. 4A). Spontaneous and optogenetically evoked spikes were observed under both 1P and 2P imaging (Fig. 4, B to E). The spike-triggered average spike waveforms were similar under 1P and 2P excitation, consistent with the view that both excitation modes populated the same voltage-sensitive photocycle intermediate states (Fig. 4F). The spike-triggered average waveforms and amplitudes were also similar for spontaneous and optogenetically evoked spikes, confirming that the 488-nm illumination did not substantially affect the GEVI performance, under either 1P or 2P voltage imaging conditions (Fig. 4F).

We compared 1P and 2P recordings from n = 8 cells, four mice. The average 1P voltage sensitivity was slightly better than the 2P sensitivity, but this did not reach statistical significance (P = 0.18; Fig. 4G). We also calculated the signal-to-noise ratio (SNR; ratio of spike height to baseline noise) for each recording and plotted this against the mean brightness (Fig. 4H). On a log-log plot, the 2P and 1P data fell along the same line, with a slope of 0.42 (95% confidence bounds: 0.37 to 0.47; R^2 = 0.87). This result is close to the shot noise limit (slope = 0.5). Thus, the greater SNR of the 1P recordings was attributed mainly to the increased fluorescence brightness under 1P excitation.

DISCUSSION

The absence of 2P voltage sensitivity with FRET-opsin reporters has long been a barrier in the field of voltage imaging. Here, we show that 2P voltage imaging with FRET-opsin GEVIs is feasible if the illumination populates the voltage-sensitive photocycle intermediates. Achieving this goal required selecting a 2P excitation wavelength (1135 nm) that efficiently populated the intermediate state and a dye that was efficiently excited at this wavelength while also undergoing efficient FRET with the opsin, and applying scan patterns which revisited each molecule frequently enough to overcome relaxation of the voltage-sensitive intermediates. These results open the door to 2P voltage imaging in vivo with FRET-opsin GEVIs.

Our photophysical studies point to strategies for rational improvement of both 1P and 2P FRET-opsin GEVIs and voltage imaging systems. For instance, there may be other dyes whose excitation peak better matches the peak of the 2P opsin sensitization spectrum while still engaging in productive FRET with the voltage-sensitive states. However, to be practically useful, dyes must also show good bioavailability in vivo, high 2P absorption cross sections, and good photostability. Protein engineering efforts to slow the kinetics of relaxation of the voltage-sensitive states could also enhance voltage sensitivity.

Our photophysical studies also suggest illumination strategies to improve 2P voltage imaging. The light that drives the GEVI into the voltage-sensitive states does not need to be the same as the light that activates the fluorescence of the attached fluorophore. For example,

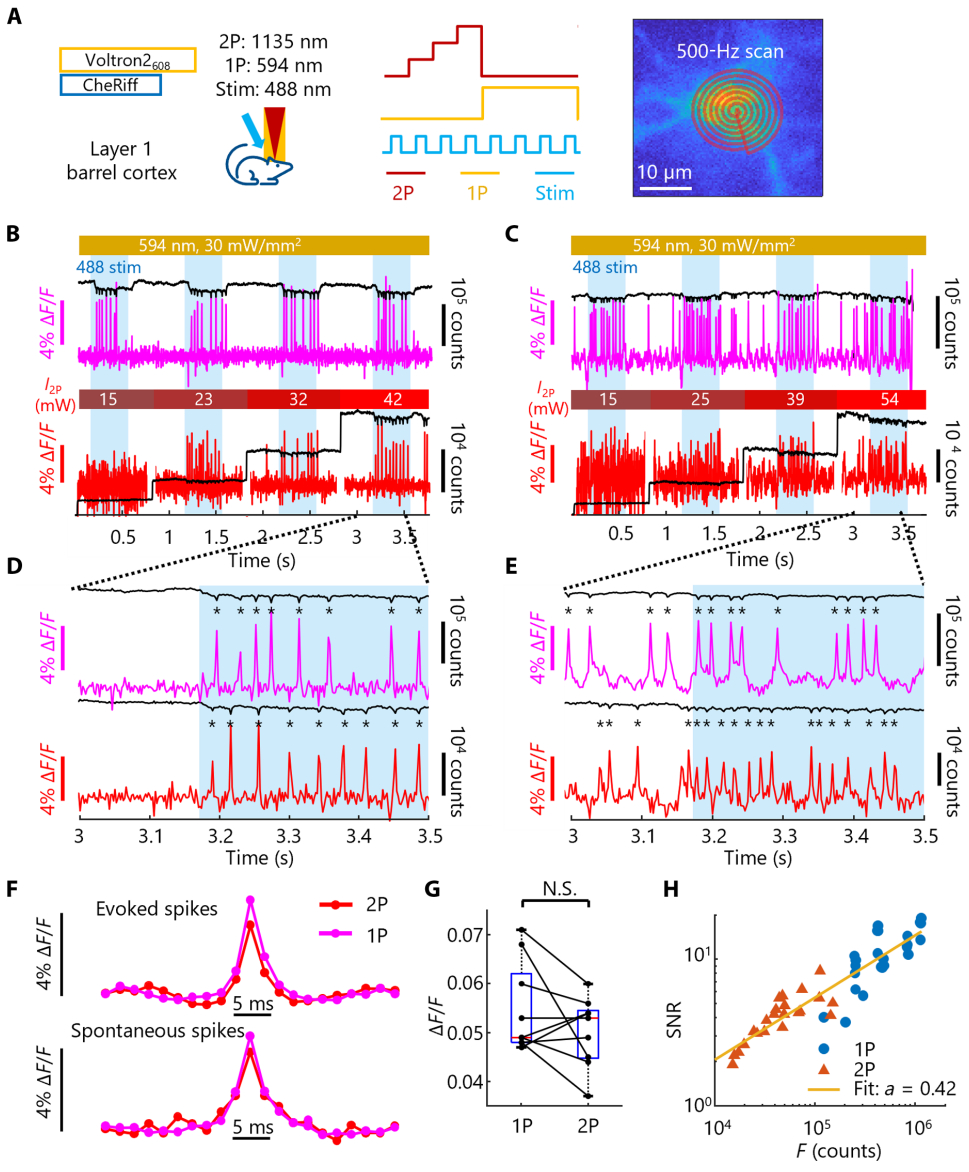

Fig. 4. 2P voltage imaging with Voltron2$_{608}$ in vivo. (**A**) Cre-dependent Voltron2 and CheRiff were coexpressed by adeno-associated virus injection in the layer 1 barrel cortex of *Ndnf-Cre* mice and imaged through a cranial window (Materials and Methods). Neurons were imaged under a 2P spiral scan (1135 nm, 500-Hz scan frequency, 15 to 54 mW) and then 1P targeted illumination (594 nm, 30 mW/mm^2). Blue light pulses (1.5 mW/mm^2) evoked activity. (**B** and **C**) Representative fluorescence traces (left axis, detrended Δ*F*/*F*; right axis, *F*) of two cells from two mice with 1P (top) and 2P (bottom) excitation. (**D** and **E**) Enlarged views of the traces showing individual spontaneous and optogenetically evoked spikes (marked with asterisks). (**F**) Spike-triggered average traces from (C). Blue light evoked spikes ($N_{1p} = 46$ and $N_{2p} = 43$) and spontaneous spikes ($N_{1p} = 18$ and $N_{2p} = 13$) from the recording shown in (C) showed similar amplitudes and widths. (**G**) Average spike heights for paired 1P and 2P recordings from the same cells were not significantly different ($n = 8$ cells, $P = 0.18$). (**H**) SNR versus fluorescence (counts per cell per frame) for each recorded cell under different illumination intensities ($n = 8$ cells). The SNR and fluorescence showed a power-law relationship with exponent $a = 0.42 \pm 0.05$ (95% confidence interval; $R^2 = 0.87$), close to the shot noise–limited SNR ($a = 0.5$). Deviation from shot noise–limited SNR in vivo is likely due to contributions from background fluorescence, brain motion, and blood flow.

one might rapidly interleave 1P flood illumination to populate the voltage-sensitive states and 2P illumination to probe the voltage-sensitive fluorescence. Interleaved 1P photosensitization and 2P imaging might allow 2P voltage imaging with more flexibility on wavelength and scan pattern than in the present embodiment where the 2P illumination serves both functions.

2P voltage imaging still faces difficulties as a practical tool for in vivo neural imaging. We recently compared the power budgets of 1P and 2P excitation: To achieve useful count rates for voltage imaging with a standard 80-MHz source, 2P excitation requires ~10^4-fold greater power per cell compared to 1P excitation (*39*). The maximum biologically safe laser power for 2P voltage imaging can be set by either average or peak illumination intensity. The time- and space-average power into the sample should avoid temperature rises greater than a few degrees Celsius (5°C can induce permanent damage, but smaller temperature rises may alter neural firing patterns) (*42*). This

typically requires that the total power be < ~200 mW. The peak intensity at the laser focus should not exceed ~1 nJ per pulse, the saturation intensity of most fluorophores (*43*). At higher intensities, nonlinear photodamage might occur.

Our brightest 2P voltage recording was obtained at a power of just under 10 mW (0.125 nJ per pulse at 80 MHz), which induced bleaching with a time constant as short as 2.5 s (with some variation between measurements). For a thermal damage limit of ~200 mW, the total number of cells that can be imaged simultaneously is thus <20. 2P fluorescence may be increased while keeping power constant by increasing peak pulse energy and decreasing laser repetition rate. However, the diffraction-limited focal energy must remain below the photochemical damage threshold of ~1 nJ per pulse. We discuss the optical and molecular constraints on 2P voltage imaging in detail in (*39*).

Our results also have important implications for use of Voltron2 under 1P excitation. For very-long-term recordings, a natural inclination is to decrease the illumination intensity to avoid photobleaching or phototoxicity. However, our results show that this strategy may unintentionally lead to a loss of voltage sensitivity. A better strategy would be to interleave epochs of intense (>10 mW/mm^2) illumination with epochs of darkness. Similarly, for voltage imaging of large samples (e.g., an entire mouse heart), the excitation intensities may be low, leading to a loss of voltage sensitivity. To preserve sensitivity, one should either make an array of focal spots or apply intermittent high-intensity illumination.

The complex photophysics of the FRET-opsin GEVIs suggest that future protein engineering efforts should be accompanied, at a minimum, by a quantification of intensity-dependent voltage sensitivity. An interesting avenue for future explorations would be to determine the photocycle basis for the intensity-dependent changes in voltage sensitivity and voltage step-response waveforms shown in Figs. 1 and 2.

MATERIALS AND METHODS

Genetic constructs

Voltron1 and Voltron2 plasmids were obtained from Addgene (nos. 119033 and 172909, respectively). For lentiviral transduction, the Voltron sequence was cloned into a lentiviral backbone with a cytomegalovirus promoter using standard Gibson Assembly. Briefly, the vector was linearized by double digestion using restriction enzymes (New England Biolabs). DNA fragments were generated by polymerase chain reaction amplification and then fused with the backbones using a NEBuilder HiFi DNA assembly kit (New England Biolabs). Resulting plasmids were verified by sequencing (GeneWiz).

For experiments in neurons, we coexpressed Voltron2 with a blue-shifted channelrhodopsin, CheRiff, by a self-cleaving p2a linker. For in vivo experiments, we generated a plasmid with soma-localized Voltron2 and soma-localized CheRiff under the hSyn promoter and flanked by LoxP sites for Cre recombinase–dependent expression. The genes were cloned into an adeno-associated virus (AAV) backbone using standard Gibson Assembly. AAV was produced by UNC Neurotools using the supplied plasmids.

HEK cell culture

HEK-293T cells were maintained in tissue culture–treated culture dishes (Corning) at 37°C and 5% CO_2 in Dulbecco's modified Eagle's medium supplemented with 10% fetal bovine serum, 1% GlutaMax-I, penicillin (100 U/ml), and streptomycin (100 mg/ml). For each imaging experiment, cells in one 35-mm dish were either transiently transfected with the construct to be imaged using TransIT-293 lipofection reagent (Mirus Bio) or virally transduced with a lentivirus. We saw no difference in voltage sensitivity or photophysics between the lipofected and virally transduced HEK cells. For lipofection, the construct was diluted 1:5 with an empty pUC19 vector (New England Biolabs) and then transfected with 7.5 μl of TransIT-293 and 2.5 μg of DNA. Cells were replated 36 to 60 hours after transfection on glass-bottom dishes (Cellvis, catalog no. D35-14-1.5-N) that were previously coated in poly-D-lysine to aid in cell adhesion.

Lentiviral transduction

All the lentivirus preparations were made in house. HEK-293T cells were cotransfected with the second-generation packaging plasmid psPAX2 (Addgene no. 12260), envelope plasmid VSV-G (Addgene no. 12259), and transfer plasmids at a ratio of 9:4:14. For small batches, 5.6 μg of total plasmids for a small culture (300k cells in a 35-mm dish) gave a sufficient yield of lentivirus. Lentivirus was not further concentrated. For lentiviral transduction, 100 μl of lentivirus was added to a single 35-mm dish. After 48 to 60 hours, cells were either replated onto glass for imaging or split and replated on 35-mm plastic dishes for continued growth. Virally transduced cultures could be used for up to three passages after transduction. For all experiments, imaging was performed 12 to 24 hours after replating on glass.

Electrophysiology and buffers

Half an hour before imaging, the appropriate JF-HaloTag ligand dye was added to the medium in each dish of cells to a final concentration of 100 nM. Immediately before imaging, the medium was removed, and the cells were rinsed and then covered with dye-free extracellular (XC) buffer. The XC buffer contained 125 mM NaCl, 2.5 mM KCl, 3 mM $CaCl_2$, 1 mM $MgCl_2$, 15 mM Hepes, and 20 mM glucose, which was adjusted with NaOH to a pH of 7.3 and with sucrose to an osmolality of 305 to 310 mosmol, as measured by a vapor-pressure osmometer (Wescor). Filamented patch pipettes were pulled using an automated puller (Sutter P-1000) to a tip resistance of ~6 × 10^6 ohms and were filled with an intracellular buffer containing 6 mM NaCl, 130 mM K-aspartate, 2 mM $MgCl_2$, 5 mM $CaCl_2$, 11 mM EGTA, and 10 mM Hepes, with pH adjusted to 7.2 by KOH (*44*). A whole-cell voltage clamp was acquired using a modified syringe to manipulate pressure, following Li (*44*).

Microscope and illumination control

1P imaging experiments were performed on a custom-built inverted microscope with a computer-controlled patch amplifier (Axon Instruments, Multiclamp 700B). Once a whole-cell patch was established, acquisition was controlled using custom MATLAB/C++ acquisition software (www.luminosmicroscopy.com/). The illumination path contained a 594-nm laser (Hübner Photonics, Cobolt Mambo) and a 561-nm laser (Hübner Photonics, Cobolt Jive). The laser outputs were modulated using a multichannel acousto-optic tunable filter (Gooch & Housego, TF525-250-6-3-GH18A with an MSD040-150 driver), and imaging was performed through a high–numerical aperture (NA) 60× water-immersion objective (Olympus UPLSAPO60XW, 0.28-mm working distance, NA = 1.2) onto a scientific complementary metal-oxide semiconductor (sCMOS) camera (Hamamatsu, ORCA-Flash 4.0). Imaging of JF_{549} and JF_{608} was performed

through a 488/561/633-nm triband dichroic mirror (Chroma) and a 405/488/594-nm triband dichroic mirror (Semrock), respectively. A 594-nm long-pass emission filter was used for both dyes (Semrock, BLP01-594R-25). Electrical waveforms and measurements were transduced through a computer-controlled data acquisition device (National Instruments, PCIe-6343). The sample was placed on a two-axis motorized stage (Ludl Electronic Products, MAC6000), and a three-axis micromanipulator was used for patch pipette control (Sutter, MP-285).

2P imaging experiments were performed on a custom-built upright microscope equipped with 1P and 2P illumination paths, a shared emission path to an sCMOS camera (Hamamatsu, ORCA-Flash 4.0), and a computer-controlled patch amplifier (Axon Instruments, Axopatch 200B). An 80-MHz tunable ultrafast laser (Spectra-Physics, InSight DeepSee) was modulated using an electro-optic modulator (ConOptics, 350-80-02 with a 302RM driver) and directed using a pair of galvanometric mirrors (Cambridge Technologies 6215H with a 671HP driver). The 488-nm (Coherent OBIS 488-100 LS), 532-nm (Laserglow LLS-05320PFM-00159-01), and 594-nm (Hübner Photonics Cobolt Mambo 0594-04-01-0100-500) lasers were combined and independently modulated using a multichannel acousto-optic tunable filter (Gooch & Housego PCAOM NI-VIS with an MSD040-150 driver). The 1P lasers were patterned using a digital micromirror device (Vialux V-7001). Imaging of HEK cells was performed through a high-NA 25× water-immersion objective (Olympus XLPLN25X-WMP2, 2-mm working distance, NA = 1.05).

In vivo imaging was performed through a high-NA 25× water-immersion objective (Olympus XLPLN25XSVMP2, 4-mm working distance, NA = 1; Olympus XLPLN25XWMP2, 2-mm working distance, NA = 1.05). A 785-nm long-pass dichroic mirror (Semrock Di03-r785-t3) separated the 2P excitation from the 1P and imaging paths. A 594 nm long-pass dichroic mirror (Semrock Di03-r594-t3) separated the 1P excitation light from the imaging path. Emission filters at 628/40 and 593/40 were used for imaging of JF_{608} and JF_{549}, respectively. Electrical waveforms and measurements were transduced through a computer-controlled data acquisition device (National Instruments, PCIe-6363). Galvo control and feedback waveforms were transduced through a second computer-controlled data acquisition device (National Instruments, PCIe-6343). The sample was placed on a motorized two-axis state, with focus controlled by objective displacement and a three-axis micromanipulator used for patch pipette control (Sutter MPC-200 controller with an MPC-78 stage and MP-285 manipulators).

Camera scaling was calibrated using a stage micrometer (Thorlabs, R1L3S2P), and illumination powers were calibrated using a power meter (Thorlabs, PM400) with either a photodiode (Thorlabs, S170C) or a thermal (Thorlabs, S175C) slide power sensor for 1P and 2P imaging, respectively.

Animals

All animal procedures adhered to the National Institutes of Health Guide for the care and use of laboratory animals and were approved by the Harvard University Institutional Animal Care and Use Committee under protocol 12-18-3.

Cranial window surgery

Surgeries were conducted on NDNF-cre X NPY-GFP mice of both sexes, following the protocol outlined in (*45*). The surgical procedure began by exposing the skull, followed by a 3-mm circular craniotomy at coordinates 3.3 to 3.4 mm lateral and 1.6 caudal relative to the bregma. The craniotomy was made using a dental drill. Following this, a stack of one 5-mm and two 3-mm round cover glass (Thomas Scientific, 1217N66), preglued by optical glue (Norland 61), was inserted into the opening. All subsequent experimental procedures were carried out at least 1 week after surgery, ensuring that the health of each mouse was stable.

AAV injection

Following craniotomy, AAV (final titer, ~4×10^{12} genome copies/ml) was injected at a rate of 45 nl/min using a home-pulled micropipette (Sutter P-1000 pipette puller) mounted in a microinjection pump (World Precision Instruments Nanoliter 2010) controlled by a microsyringe pump controller (World Precision Instruments Micro4). The micropipette was positioned using a stereotaxic instrument (Sutter Instruments).

In vivo imaging

JF_{608}-HaloTag ligand solution was first prepared as previously described (*41*) and was then retro-orbitally delivered 24 hours before the imaging session. In vivo imaging was performed under light anesthesia following a previously described protocol (*46*). Briefly, mice were subcutaneously injected with chlorprothixene (0.2 mg/ml; 5 μl/g body weight) 30 min before the imaging session. During imaging, isoflurane (0.4 to 0.7%) was administered to maintain a semi-awake state, characterized by minimal sedation with occasional body movements. Mice were head fixed under the upright microscope using a titanium head plate. Eyes were kept moist using ophthalmic eye ointment. The body temperature was continuously monitored and maintained at 37°C using a heating pad (WPI, ATC-2000). A typical imaging session lasted 1 to 2 hours, after which the animals quickly recovered within 5 min and were returned to their home cage.

Analysis

All analyses were performed in MATLAB. Analysis of 1P-only experiments (Figs. 1 and 2) began with manual selection of a membrane region of interest (ROI) from each cell. The same ROI was used for all experiments from a given cell. A time trace of fluorescence was extracted by equal-weighted averaging of photon counts over the selected ROI, followed by subtraction of the mean counts from a background region selected near the cell. This time trace was smoothed with a moving mean filter of window of 10 ms, except for that displayed in Fig. 1 (D to G), where it was smoothed with a moving mean filter of window of 20 ms. Photobleaching was corrected using a biexponential fit to each illumination epoch. For 1P experiments in Figs. 1 and 2, this fit provided the baseline from which values of $\Delta F/F$ were calculated.

For the plots of $\Delta F/F$ versus V in Fig. 1, the baseline fluorescence F was determined during holding periods between defined steps. During these holding periods, the voltage was clamped at −70 mV. The voltage was stepped to a series of different values, including one "step" to −70 mV. The fluorescence during the measurement epochs had some noise, leading to the small deviations of ΔF from zero in the −70-mV data points.

For the data in Fig. 3, values of $\Delta F/F$ were determined using a regression-based approach, designed to be insensitive to intracellular fluorescence [introduced in (*9*)]. First, the fluorescence trace at each pixel was corrected for photobleaching, as above. Next, a pixel-wise scatter plot of ΔF versus F was created over all pixels in a manually selected ROI. The upper hull of this scatter plot corresponds to pixels with the smallest contribution from voltage-insensitive fluorescence. The slope of this upper hull was used to determine $\Delta F/F$.

Neural spike recordings were detrended by smoothing the data with a moving mean filter of width of 50 ms. This produced a smooth baseline from which $\Delta F/F$ could be calculated for the raw fluorescence trace. The signal was inverted, and then the noise σ was estimated as the range from the 10th to 40th percentile of the data. The spike-detection threshold was set as the mean + 3σ. For each cell, the same threshold was applied for both 1P and 2P imaging. The voltage sensitivity was determined by averaging the spikes from each cell. The logarithm of the SNR and per-cell counts was taken, and a linear fit was performed using MATLAB's curve fitting toolbox. Significance of paired conditions was calculated using a two-tailed paired sample *t* test using MATLAB's machine learning and statistics toolbox.

REFERENCES AND NOTES

1. Y. Adam, All-optical electrophysiology in behaving animals. *J. Neurosci. Methods* **353**, 109101 (2021).
2. A. S. Abdelfattah, J. Zheng, A. Singh, Y.-C. Huang, D. Reep, G. Tsegaye, A. Tsang, B. J. Arthur, M. Rehorova, C. V. L. Olson, Y. Shuai, L. Zhang, T.-M. Fu, D. E. Milkie, M. V. Moya, T. D. Weber, A. L. Lemire, C. A. Baker, N. Falco, Q. Zheng, J. B. Grimm, M. C. Yip, D. Walpita, M. Chase, L. Campagnola, G. J. Murphy, A. M. Wong, C. R. Forest, J. Mertz, M. N. Economo, G. C. Turner, M. Koyama, B.-J. Lin, E. Betzig, O. Novak, L. D. Lavis, K. Svoboda, W. Korff, T.-W. Chen, E. R. Schreiter, J. P. Hasseman, I. Kolb, Sensitivity optimization of a rhodopsin-based fluorescent voltage indicator. *Neuron* **111**, 1547–1563.e9 (2023).
3. U. L. Böhm, Y. Kimura, T. Kawashima, M. B. Ahrens, S.-i. Higashijima, F. Engert, A. E. Cohen, Voltage imaging identifies spinal circuits that modulate locomotor adaptation in zebrafish. *Neuron* **110**, 1211–1222.e4 (2022).
4. Y. Adam, J. J. Kim, S. Lou, Y. Zhao, M. E. Xie, D. Brinks, H. Wu, M. A. Mostajo-Radji, S. Kheifets, V. Parot, S. Chettih, K. J. Williams, B. Gmeiner, S. L. Farhi, L. Madisen, E. K. Buchanan, I. Kinsella, D. Zhou, L. Paninski, C. D. Harvey, H. Zeng, P. Arlotta, R. E. Campbell, A. E. Cohen, Voltage imaging and optogenetics reveal behaviour-dependent changes in hippocampal dynamics. *Nature* **569**, 413–417 (2019).
5. J. M. Kralj, D. R. Hochbaum, A. D. Douglass, A. E. Cohen, Electrical spiking in *Escherichia coli* probed with a fluorescent voltage indicating protein. *Science* **333**, 345–348 (2011).
6. W. Akemann, H. Mutoh, A. Perron, Y. K. Park, Y. Iwamoto, T. Knöpfel, Imaging neural circuit dynamics with a voltage-sensitive fluorescent protein. *J. Neurophysiol.* **108**, 2323–2337 (2012).
7. Y. Gong, C. Huang, J. Z. Li, B. F. Grewe, Y. Zhang, S. Eismann, M. J. Schnitzer, High-speed recording of neural spikes in awake mice and flies with a fluorescent voltage sensor. *Science* **350**, 1361–1366 (2015).
8. J. D. Wong-Campos, P. Park, H. Davis, Y. Qi, H. Tian, D. G. Itkis, D. Kim, J. B. Grimm, S. E. Plutkis, L. Lavis, A. E. Cohen, Voltage dynamics of dendritic integration and back-propagation in vivo. bioRxiv 2023.05.25.542363 [Preprint] (2023). https://doi.org/10.1101/2023.05.25.542363.
9. A. T. Landau, P. Park, J. D. Wong-Campos, H. Tian, A. E. Cohen, B. L. Sabatini, Dendritic branch structure compartmentalizes voltage-dependent calcium influx in cortical layer 2/3 pyramidal cells. *eLife* **11**, e76993 (2022).
10. P. Park, D. Wong-Campos, D. G. Itkis, Y. Qi, H. Davis, J. B. Grimm, S. E. Plutkis, L. Lavis, A. E. Cohen, Dendritic voltage imaging reveals biophysical basis of associative plasticity rules. bioRxiv 2023.06.02.543490 [Preprint] (2023). https://doi.org/10.1101/2023.06.02.543490.
11. B. Z. Jia, Y. Qi, J. D. Wong-Campos, S. G. Megason, A. E. Cohen, A bioelectrical phase transition patterns the first vertebrate heartbeats. *Nature* **622**, 149–155 (2023).
12. L. Sacconi, L. Silvestri, E. C. Rodríguez, G. A. B. Armstrong, F. S. Pavone, A. Shrier, G. Bub, KHz-rate volumetric voltage imaging of the whole Zebrafish heart. *Biophys. Rep.* **2**, 100046 (2022).
13. N. Azimi Hashemi, A. C. F. Bergs, C. Schüler, A. R. Scheiwe, W. Steuer Costa, M. Bach, J. F. Liewald, A. Gottschalk, Rhodopsin-based voltage imaging tools for use in muscles and neurons of *Caenorhabditis elegans*. *Proc. Natl. Acad. Sci. U.S.A.* **116**, 17051–17060 (2019).
14. J. M. Kralj, A. D. Douglass, D. R. Hochbaum, D. Maclaurin, A. E. Cohen, Optical recording of action potentials in mammalian neurons using a microbial rhodopsin. *Nat. Methods* **9**, 90–95 (2012).
15. K. D. Piatkevich, E. E. Jung, C. Straub, C. Linghu, D. Park, H.-J. Suk, D. R. Hochbaum, D. Goodwin, E. Pnevmatikakis, N. Pak, T. Kawashima, C.-T. Yang, J. L. Rhoades, O. Shemesh, S. Asano, Y.-G. Yoon, L. Freifeld, J. L. Saulnier, C. Riegler, F. Engert, T. Hughes, M. Drobizhev, B. Szabo, M. B. Ahrens, S. W. Flavell, B. L. Sabatini, E. S. Boyden, A robotic multidimensional directed evolution approach applied to fluorescent voltage reporters. *Nat. Chem. Biol.* **14**, 352–360 (2018).
16. D. R. Hochbaum, Y. Zhao, S. Farhi, N. Klapoetke, C. A. Werley, V. Kapoor, P. Zou, J. M. Kralj, D. Maclaurin, N. Smedemark-Margulies, J. Saulnier, G. Boulting, Y. Cho, M. Melkonian, G. K.-S. Wong, D. J. Harrison, V. N. Murthy, B. Sabatini, E. S. Boyden, R. E. Campbell, A. E. Cohen, All-optical electrophysiology in mammalian neurons using engineered microbial rhodopsins. *Nat. Methods* **11**, 825–833 (2014).
17. P. Zou, Y. Zhao, A. D. Douglass, D. R. Hochbaum, D. Brinks, C. A. Werley, D. J. Harrison, R. E. Campbell, A. E. Cohen, Bright and fast multicoloured voltage reporters via electrochromic FRET. *Nat. Commun.* **5**, 4625 (2014).
18. Y. Gong, M. J. Wagner, J. Z. Li, M. J. Schnitzer, Imaging neural spiking in brain tissue using FRET-opsin protein voltage sensors. *Nat. Commun.* **5**, 3674 (2014).
19. M. Kannan, G. Vasan, S. Haziza, C. Huang, R. Chrapkiewicz, J. Luo, J. A. Cardin, M. J. Schnitzer, V. A. Pieribone, Dual-polarity voltage imaging of the concurrent dynamics of multiple neuron types. *Science* **378**, eabm8797 (2022).
20. A. S. Abdelfattah, T. Kawashima, A. Singh, O. Novak, H. Liu, Y. Shuai, Y.-C. Huang, L. Campagnola, S. C. Seeman, J. Yu, J. Zheng, J. B. Grimm, R. Patel, J. Friedrich, B. D. Mensh, L. Paninski, J. J. Macklin, G. J. Murphy, K. Podgorski, B.-J. Lin, T.-W. Chen, G. C. Turner, Z. Liu, M. Koyama, K. Svoboda, M. B. Ahrens, L. D. Lavis, E. R. Schreiter, Bright and photostable chemigenetic indicators for extended in vivo voltage imaging. *Science* **365**, 699–704 (2019).
21. A. S. Abdelfattah, R. Valenti, J. Zheng, A. Wong, GENIE Project Team, K. Podgorski, M. Koyama, D. S. Kim, E. R. Schreiter, A general approach to engineer positive-going eFRET voltage indicators. *Nat. Commun.* **11**, 3444 (2020).
22. S. Liu, C. Lin, Y. Xu, H. Luo, L. Peng, X. Zeng, H. Zheng, P. R. Chen, P. Zou, A far-red hybrid voltage indicator enabled by bioorthogonal engineering of rhodopsin on live neurons. *Nat. Chem.* **13**, 472–479 (2021).
23. M.-P. Chien, D. Brinks, G. Testa-Silva, H. Tian, F. P. Brooks III, Y. Adam, B. Bloxham, B. Gmeiner, S. Kheifets, A. E. Cohen, Photoactivated voltage imaging in tissue with an archaerhodopsin-derived reporter. *Sci. Adv.* **7**, eabe3216 (2021).
24. S. Chamberland, H. H. Yang, M. M. Pan, S. W. Evans, S. Guan, M. Chavarha, Y. Yang, C. Salesse, H. Wu, J. C. Wu, T. R. Clandinin, K. Toth, M. Z. Lin, F. St-Pierre, Fast two-photon imaging of subcellular voltage dynamics in neuronal tissue with genetically encoded indicators. *eLife* **6**, e25690 (2017).
25. Z. Liu, X. Lu, V. Villette, Y. Gou, K. L. Colbert, S. Lai, S. Guan, M. A. Land, J. Lee, T. Assefa, D. R. Zollinger, M. M. Korympidou, A. L. Vlasits, M. M. Pang, S. Su, C. Cai, E. Froudarakis, N. Zhou, S. S. Patel, C. L. Smith, A. Ayon, P. Bizouard, J. Bradley, K. Franke, T. R. Clandinin, A. Giovannucci, A. S. Tolias, J. Reimer, S. Dieudonné, F. St-Pierre, Sustained deep-tissue voltage recording using a fast indicator evolved for two-photon microscopy. *Cell* **185**, 3408–3425.e29 (2022).
26. D. Brinks, A. J. Klein, A. E. Cohen, Two-photon lifetime imaging of voltage indicating proteins as a probe of absolute membrane voltage. *Biophys. J.* **109**, 914–921 (2015).
27. Y. Bando, M. Sakamoto, S. Kim, I. Ayzenshtat, R. Yuste, Comparative evaluation of genetically encoded voltage indicators. *Cell Rep.* **26**, 802–813.e4 (2019).
28. R. W. Hendler, R. I. Shrager, S. Bose, Theory and procedures for finding a correct kinetic model for the bacteriorhodopsin photocycle. *J. Phys. Chem. B* **105**, 3319–3328 (2001).
29. J. K. Lanyi, Bacteriorhodopsin. *Annu. Rev. Physiol.* **66**, 665–688 (2004).
30. H. Bayraktar, A. P. Fields, J. M. Kralj, J. L. Spudich, K. J. Rothschild, A. E. Cohen, Ultrasensitive measurements of microbial rhodopsin photocycles using photochromic FRET. *Photochem. Photobiol.* **88**, 90–97 (2012).
31. D. Maclaurin, V. Venkatachalam, H. Lee, A. E. Cohen, Mechanism of voltage-sensitive fluorescence in a microbial rhodopsin. *Proc. Natl. Acad. Sci. U.S.A.* **110**, 5939–5944 (2013).
32. J. Kübel, M. Chenchiliyan, S. A. Ooi, E. Gustavsson, L. Isaksson, V. Kuznetsova, J. A. Ihalainen, S. Westenhoff, M. Maj, Transient IR spectroscopy identifies key interactions and unravels new intermediates in the photocycle of a bacterial phytochrome. *Phys. Chem. Chem. Phys.* **22**, 9195–9203 (2020).
33. A. Penzkofer, A. Silapetere, P. Hegemann, Photocycle dynamics of the Archaerhodopsin 3 based fluorescent voltage sensor Archon2. *J. Photochem. Photobiol. B Biol.* **225**, 112331 (2021).
34. V. Venkatachalam, D. Brinks, D. Maclaurin, D. Hochbaum, J. Kralj, A. E. Cohen, Flash memory: Photochemical imprinting of neuronal action potentials onto a microbial rhodopsin. *J. Am. Chem. Soc.* **136**, 2529–2537 (2014).
35. J. H. Hou, V. Venkatachalam, A. E. Cohen, Temporal dynamics of microbial rhodopsin fluorescence reports absolute membrane voltage. *Biophys. J.* **106**, 639–648 (2014).
36. A. Silapetere, S. Hwang, Y. Hontani, R. G. Fernandez Lahore, J. Balke, F. V. Escobar, M. Tros, P. E. Konold, R. Matis, R. Croce, P. J. Walla, P. Hildebrandt, U. Alexiev, J. T. M. Kennis, H. Sun, T. Utesch, P. Hegemann, QuasAr Odyssey: The origin of fluorescence and its voltage sensitivity in microbial rhodopsins. *Nat. Commun.* **13**, 5501 (2022).
37. A. Penzkofer, A. Silapetere, P. Hegemann, Theoretical investigation of the photocycle dynamics of the Archaerhodopsin 3 based fluorescent voltage sensor Archon2. *J. Photochem. Photobiol. A Chem.* **437**, 114366 (2023).
38. C. Huang, J. Luo, S. J. Woo, L. A. Roitman, J. Li, V. A. Pieribone, M. Kannan, G. Vasan, M. J. Schnitzer, Dopamine-mediated interactions between short- and long-term memory dynamics. *Nature* **634**, 1141–1149 (2024).

39. F. P. Brooks III, H. C. Davis, J. D. Wong-Campos, A. E. Cohen, Optical constraints on two-photon voltage imaging. *Neurophotonics* **11**, 035007 (2024).
40. R. R. Birge, C.-F. Zhang, Two-photon double resonance spectroscopy of bacteriorhodopsin. Assignment of the electronic and dipolar properties of the low-lying $^1A^{*-}{}_g$-like and $^1B^{*+}{}_u$-like π, π^* states. *J. Chem. Phys.* **92**, 7178–7195 (1990).
41. J. B. Grimm, A. K. Muthusamy, Y. Liang, T. A. Brown, W. C. Lemon, R. Patel, R. Lu, J. J. Macklin, P. J. Keller, N. Ji, L. D. Lavis, A general method to fine-tune fluorophores for live-cell and in vivo imaging. *Nat. Methods* **14**, 987–994 (2017).
42. K. Podgorski, G. Ranganathan, Brain heating induced by near-infrared lasers during multiphoton microscopy. *J. Neurophysiol.* **116**, 1012–1023 (2016).
43. K. Charan, B. Li, M. Wang, C. P. Lin, C. Xu, Fiber-based tunable repetition rate source for deep tissue two-photon fluorescence microscopy. *Biomed. Opt. Express* **9**, 2304–2311 (2018).
44. C. Li, A reliable whole cell clamp technique. *Adv. Physiol. Educ.* **32**, 209–211 (2008).
45. G. J. Goldey, D. K. Roumis, L. L. Glickfeld, A. M. Kerlin, R. C. Reid, V. Bonin, D. P. Schafer, M. L. Andermann, Removable cranial windows for long-term imaging in awake mice. *Nat. Protoc.* **9**, 2515–2538 (2014).
46. H. Tian, H. C. Davis, J. D. Wong-Campos, P. Park, L. Z. Fan, B. Gmeiner, S. Begum, C. A. Werley, G. B. Borja, H. Upadhyay, H. Shah, J. Jacques, Y. Qi, V. Parot, K. Deisseroth, A. E. Cohen, Video-based pooled screening yields improved far-red genetically encoded voltage indicators. *Nat. Methods* **20**, 1082–1094 (2023).

Acknowledgments: We thank D. Itkis, J. Xu, M. Howell, R. F. Hayward, Y. Wang, A. Preecha, S. Begum, C. Bodden, D. Wong-Campos, B. H. Lee, and E. Perets for technical assistance and helpful discussions. **Funding:** This work was supported by NIH grants 1R01NS133755 and 1RF1NS126043 and NSF Quantum Sensing for Biophysics and Bioengineering (QuBBE) Quantum Leap Challenge Institute (QLCI) grant OMA-2121044. **Author contributions:** F.P.B., H.C.D., and A.E.C. designed the study and experiments. F.P.B., D.G., and A.E.C. wrote the manuscript with input from all authors. F.P.B. and D.G. collected the 1P data. F.P.B., D.G., and H.C.D. collected the 2P HEK-293 data. Y.Q. and P.P. prepared the AAV construct, conducted virus injection and cranial window surgery, and assisted F.P.B. and D.G. with data collection for 2P in vivo imaging. F.P.B. and D.G. performed analyses with critical input from H.C.D. and A.E.C. A.E.C. supervised the work. **Competing interests:** The authors declare that they have no competing interests. **Data and materials availability:** All data needed to evaluate the conclusions in the paper are present in the paper. Voltage imaging data are available on the DANDI archive at https://dandiarchive.org/dandiset/000988.

Submitted 1 April 2024
Accepted 4 December 2024
Published 8 January 2025
10.1126/sciadv.adp5763